Electronic Supplementary Material (ESI) for Journal of Materials Chemistry A.

Robust Molecular Dipole Induced Surface Functionalization of Inorganic Perovskites for Efficient Solar Cells

*Junming Qiu, Qisen Zhou, Donglin Jia, Yunfei Wang, Shuang Li, and Xiaoliang Zhang**

School of Materials Science and Engineering, Beihang University, Beijing 100191, China. E-mail: xiaoliang.zhang@buaa.edu.cn

Contents

Experimental Section

Materials: *N*, *N*-Dimethylformamide (DMF), dimethyl sulfoxide (DMSO), 2-propanol (IPA), chlorobenzene, acetonitrile, 4-tert-butylpyridine (t-BP) and bis(trifluoromethane)sulfonimide lithium salt (Li-TFSI) were obtained from Sigma-Aldrich. Cesium Iodide (CsI), DMAI, Spiro-OMeTAD and Co (III) bis(trifluoromethane)sulfonimide salt (FK-209) were purchased from Xian Polymer Light Technology Corp. Lead (II) iodide (PbI_2), CA-NO_2, CA-CF_3, CA, CA-OCH_3 and CA-NH_2 were purchased from TCI. All materials were used as received and without any purification.

PSC Fabrication: The laser patterned FTO glass substrate was ultrasonically cleaned with detergent, deionized water, acetone and ethanol sequentially. Then, the substrate was dried with nitrogen and further cleaned using UV ozone plasma for 30 min. To obtain a compact TiO_2 layer, a mildly acidic solution of titanium isopropoxide in ethanol was spin-coated on the top of the pre-cleaned substrate at 2000 rpm and then annealed at 500 ℃ for 1 h. The perovskite precursor solution (0.8 M) was prepared by dissolving stoichiometric CsI, PbI_2 and DMAI with 1:1:1 molar ratio in a DMF/DMSO mixed solvent (v/v:9/1). The perovskite film was prepared using a one-step spin-coating approach under dry air conditions (RH of 15±5 %). In detail, the perovskite precursor solution was spin-coated on 70 °C pre-warmed c-TiO_2/FTO substrate at 3000 rpm for 30 s with a ramping rate of 1500 rpm s^{-1}. After that, the as-coated films were immediately annealed at 70 ℃ for 2 min to obtain the transition films. Subsequently, the transition films were annealed at 210 ℃ for another 5 min to finish the crystallization of perovskites. For surface functionalization, ~100 µl of CA-based molecules in isopropanol with different concentrations (2.5, 5 and 10 mM) was spin-coated on the top surface of the perovskite film at 4000 rpm for 30 s, and then the film was annealed at 100 ℃ for 5 min to evaporate the excess solvent. The Spiro-OMeTAD layer was deposited by spin-coating at 3000 rpm for 30 s with a solution comprising of 1ml chlorobenzene, 72.3 mg spiro-OMeTAD, 30 µl t-BP, 17.5 µl Li-TFSI solution (520 mg of Li-TFSI in 1 mL acetonitrile) and 29 µl FK-209 (300 mg of Li-TFSI in 1 mL

acetonitrile). Finally, the devices were completed by evaporating 100 nm Ag electrode.

Characterizations: The SEM image was obtained using a scanning electron microscope (Zeiss SUPRA55) with an accelerating voltage of 10 kV. XRD pattern was measured with Rigaku D/max2500 using Cu Ka radiation (λ = 1.54178 Å) in an angle range of 5-60 °. The light absorption spectrum was tested using a UV-vis spectrophotometer (UV-3600, Shimadzu, Japan) and the PL spectra were performed using Ocean Optical LLS-490 fluorophotometer with an excitation wavelength of 405 nm. TRPL decay measurement was carried out using a picosecond diode laser (FLS980) with an excitation wavelength of 485 nm. The PL spectra and TRPL spectra of perovskite films were obtained with a layer stack of perovskite/glass. XPS spectra were acquired using Thermo Scientific Escalab 250Xi US with a micro-focus monochromatic Al Kα *X*-ray source. UPS analysis was conducted using Thermo escalab Ei^{+} Ultraviolet photoelectron spectrometer with He-I (21.22 eV) source as an excitation source. Versa SCAN Scanning Kelvin probe (SKP) was operated to measure the relative work function, which integrates the positioning system with the Signal Recovery lock-in circuit, the piezoelectric vibration module and the potentiometer.

The *J-V* curve of unencapsulated PSCs was recorded using a Keithley 2400 source meter with a voltage scanning rate of 100 mV/s in the ambient atmosphere. The working area of the solar cell was 0.09 cm^2, which was defined using a non-reflective metallic mask. The AM1.5G 100 mW/cm^2 illumination was supplied by a solar simulator (Enli SS-F5-3A) and before the measurement, the light intensity was calibrated using a certified silicon reference cell (Fraunhofer ISE). EQE spectrum was measured using an Enli Technology QE-R system, which consisted of a xenon lamp (QE-LD), a Czerny-Turner monochromator (QE-M110), an optical imaging system and a light intensity detection system (QE-M1). The TPV decay was conducted using Zahner Zennium CIMPS-pro electrochemical workstation. The Mott-Schottky curve was measured using the Zahner Zennium CIMPS-pro electrochemical workstation in a dark box at a bias of 0~1.2 V. The photostability of solar cells was tested using the solar cell stability

test setup (PV-S-16, Tianjin Meitong Corp., China), which was carried out under continuous 100 mW/cm^2 illumination provided by a white LED (MT-LED-70).

Computational Details: The Vienna *Ab initio* Simulation Package (VASP) was employed to carry out first-principles calculations.[1] The projected-augmented-wave (PAW) method was employed to describe the electron-ion interaction.[2] Since the use of a large supercell is significantly time-consuming by using hybrid functional with spin-orbit coupling (SOC), exchange and correlation energies were computed within the generalized gradient approximation (GGA) using the Perdew-Burke-Ernzerhof (PBE) functional neglecting SOC.[3] The DFT-PBE calculations did not make an obvious change to the band structure shape from the hybrid functional calculations and that PBE without SOC yields a similar tendency in the charge distribution, indicating that investigation of the defect passivation could not be affected by the lack of hybrid functional and SOC.[4-6] Grimme's DFT-D3 was used for dispersion correction.[7] A plane-wave basis set with an energy cutoff of 400 eV was employed in all calculations. The Pb-I surfaces were modeled by a slab consisting of 3×3 periodicity in the a-b plane with a 30 Å of vacuum along the c-axis. The surface structure of the perovskites and the molecule was optimized until the forces below 0.02 eV/Å and the energy below 1.0×10^{-5} eV. The Monkhorst-Pack *k*-point mesh of (3×3×1) was adopted for the Brillouin zone. The adsorption energies were calculated with the following equation: $E_{ad} = E_{total} - E_{perovskite} - E_{molecule}$, where E_{total} is the total energy of the adsorption configuration, $E_{perovskite}$ and $E_{molecule}$ are the energy of perovskite slab and single-molecule before interactions, respectively.

Supplementary Figures

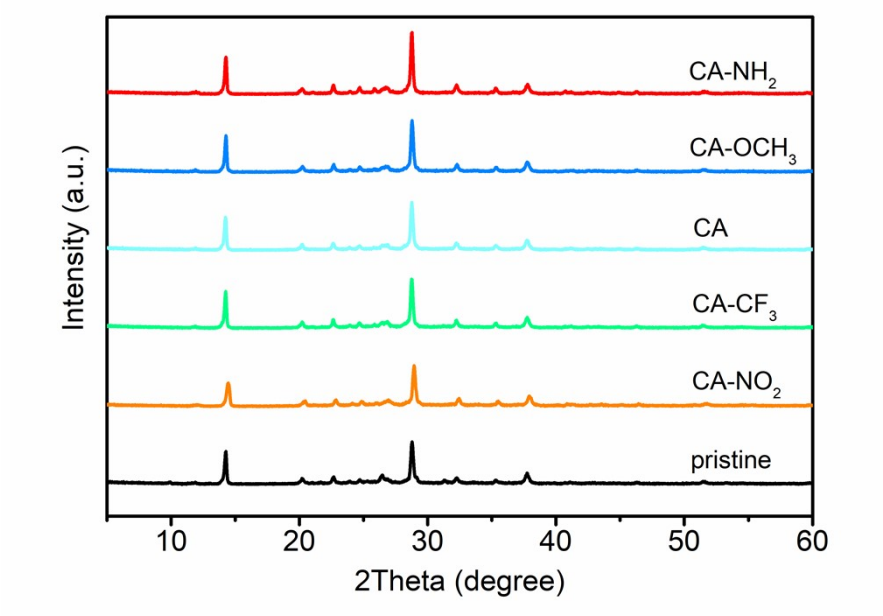

Figure S1. XRD patterns of the perovskite films without and with the surface functionalization.

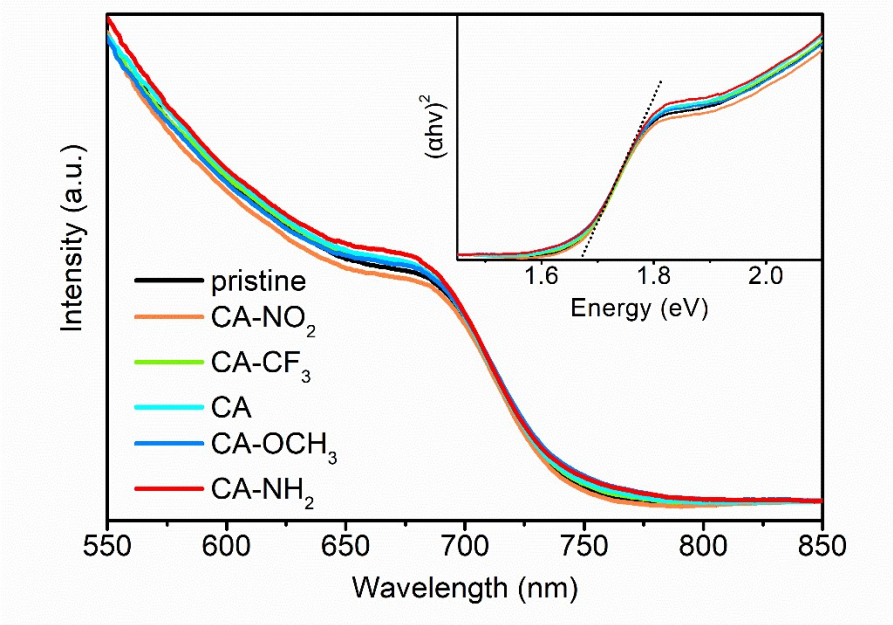

Figure S2. UV-vis spectra of the perovskite films without and with the surface functionalization.

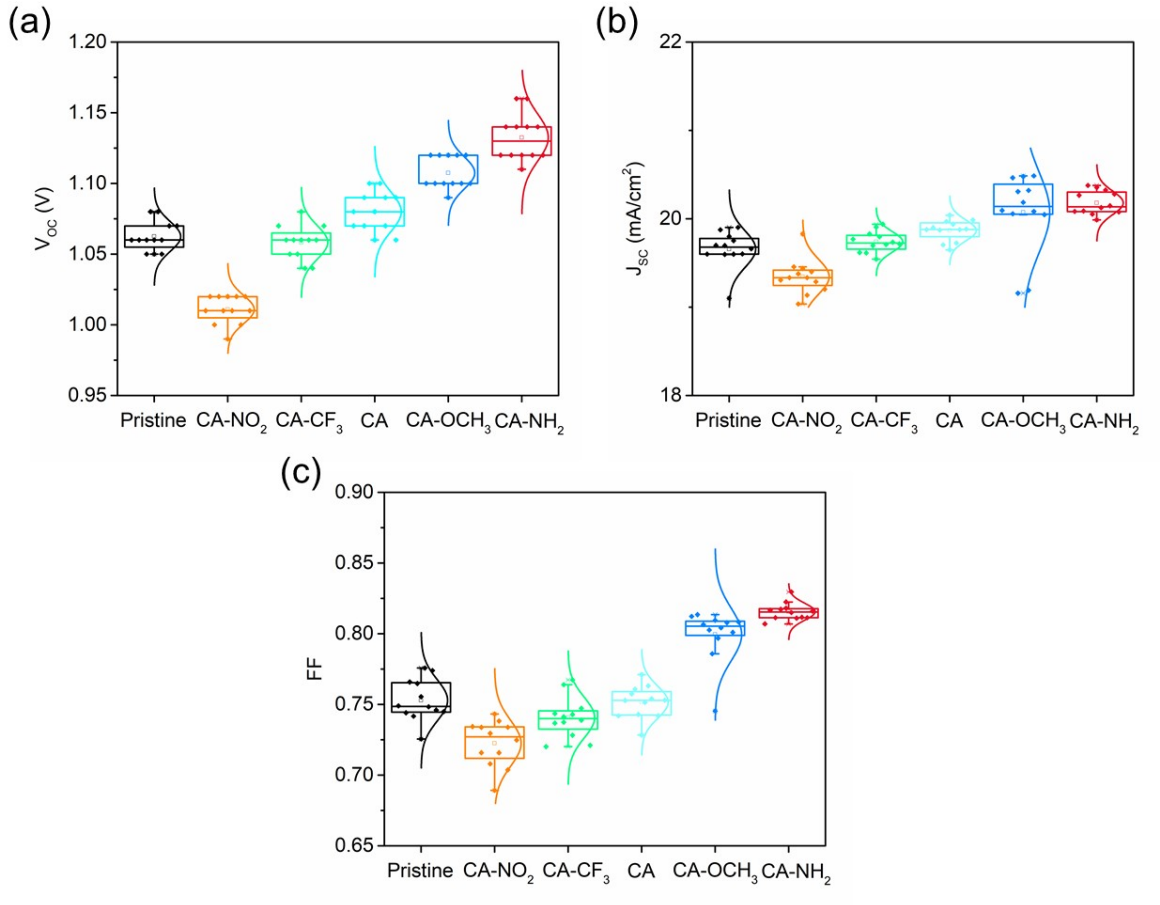

Figure S3. Photovoltaic parameters statistics of $CsPbI_3$ PSCs without and with the surface treatment using CA-based molecules. (a) V_{oc}, (b) J_{sc} and (c) FF.

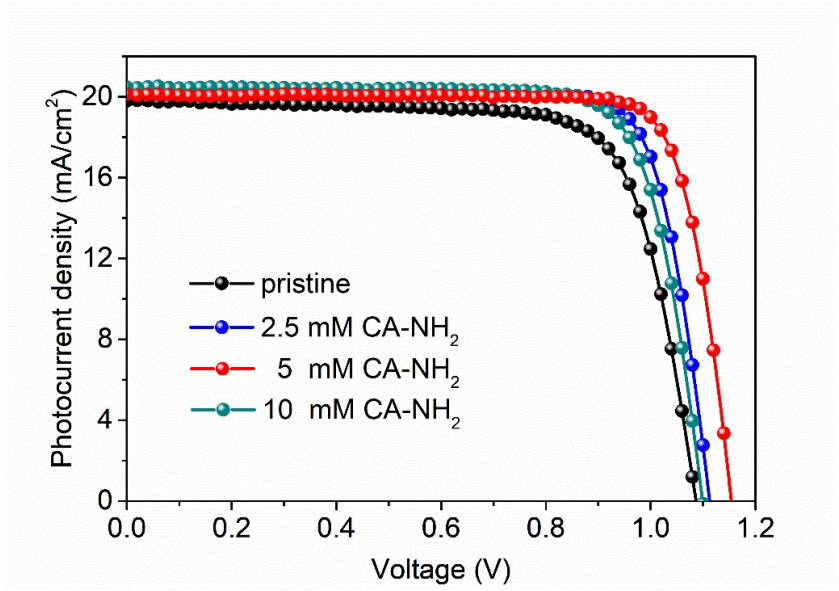

Figure S4. *J-V* curves of the CA-NH_2-based PSCs fabricated with different concentrations of CA-NH_2 molecules for the surface functionalization of inorganic perovskites.

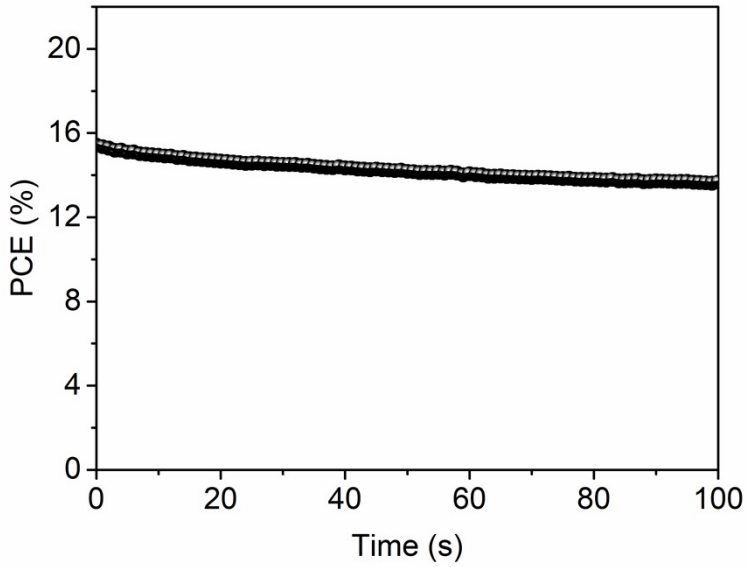

Figure S5. The stabilized power output of the pristine PSC. The test was measured under 0.9 V bias voltage.

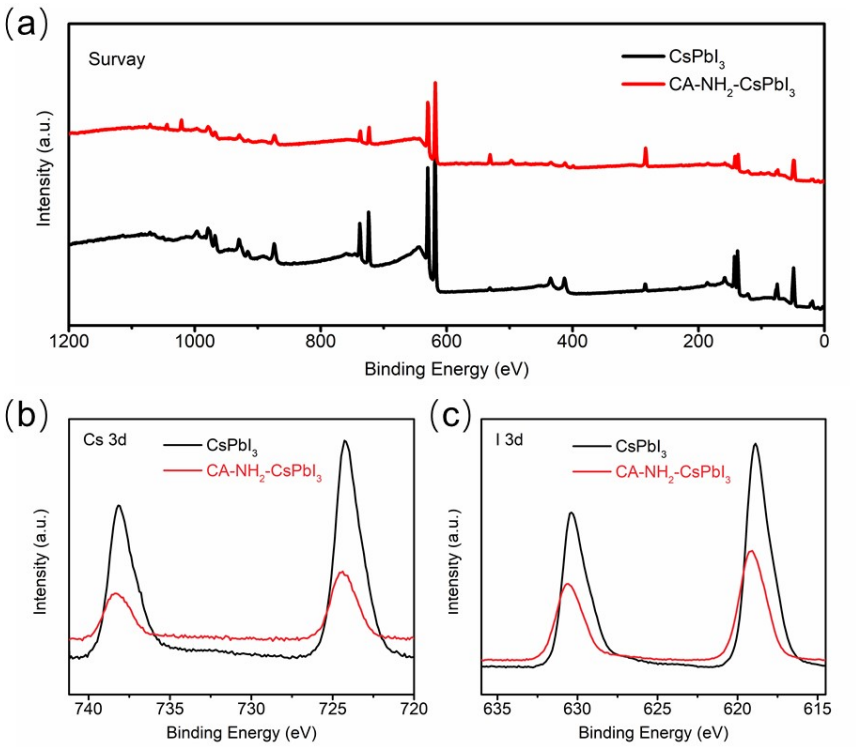

Figure S6. XPS spectra of the pristine and CA-NH_2-based perovskite films. (a) Full spectra, (b) Cs 3*d*, and (c) I 3*d* core-level spectra.

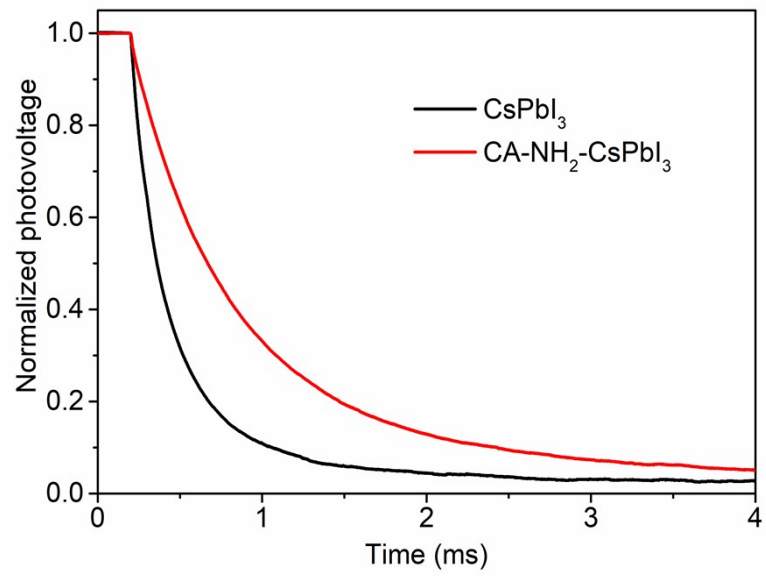

Figure S7. TPV curves of pristine and CA-NH_2-based PSCs.

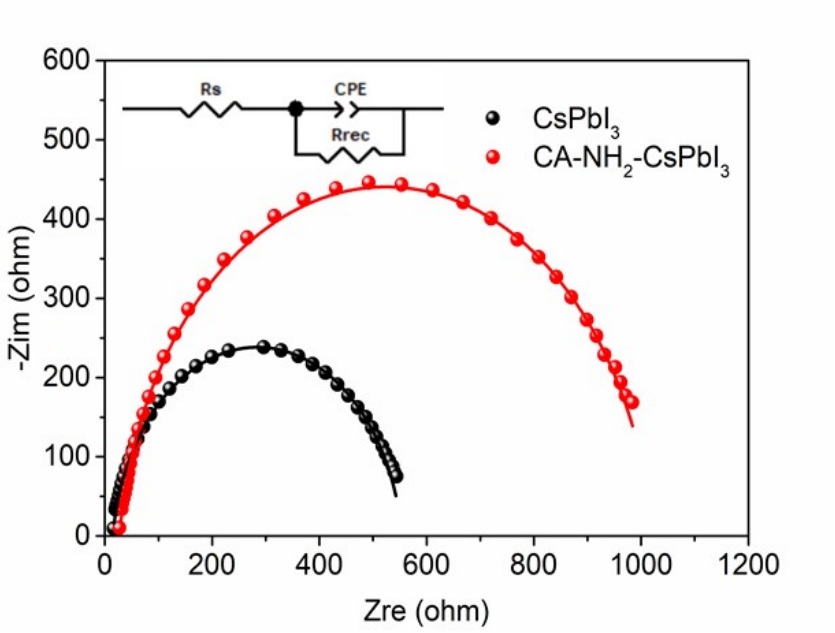

Figure S8. EIS plots of pristine and CA-NH_2-based PSCs.

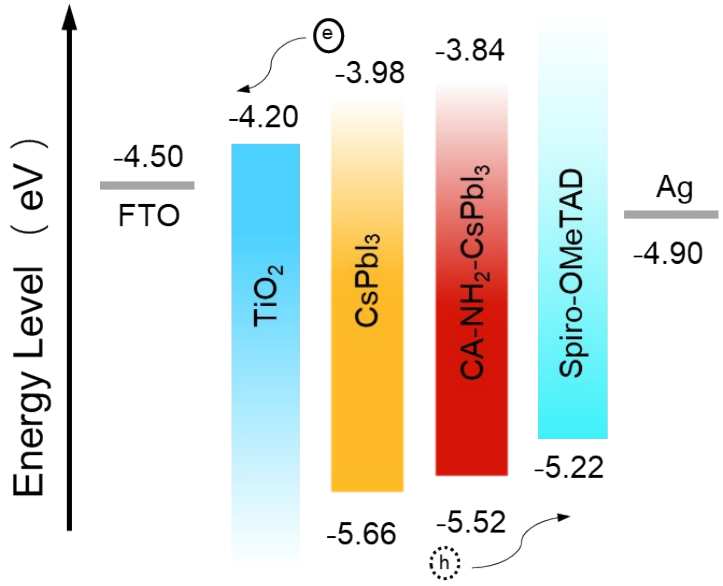

Figure S9. The energy-level diagram of each functional layer in the PSCs.

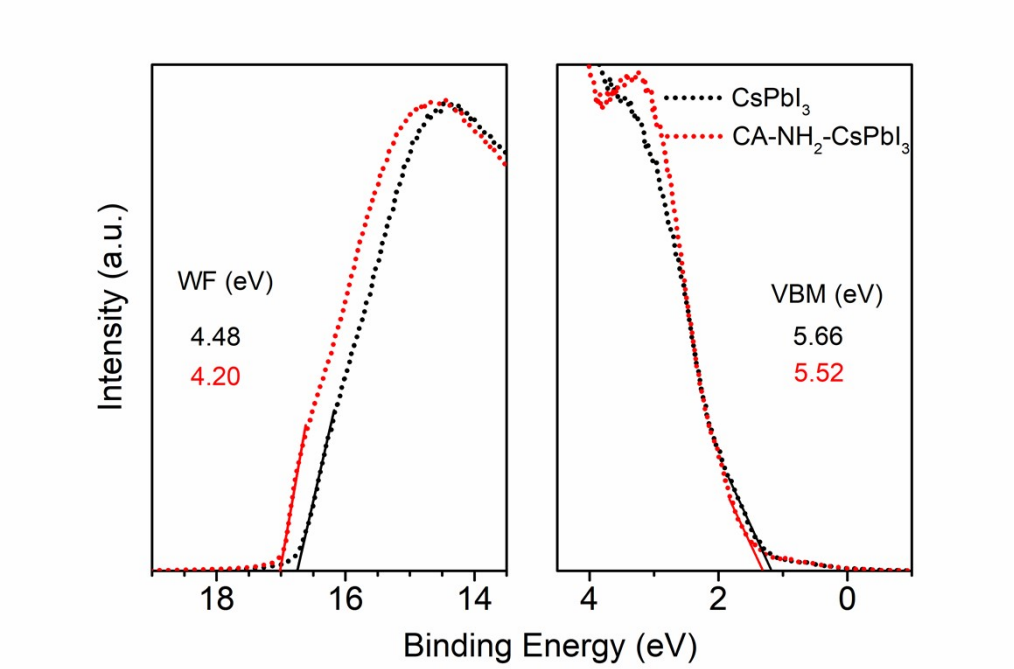

Figure S10. UPS spectra (using He-I with a photon energy of 21.22 eV) of pristine and CA-NH_2-based perovskite films.

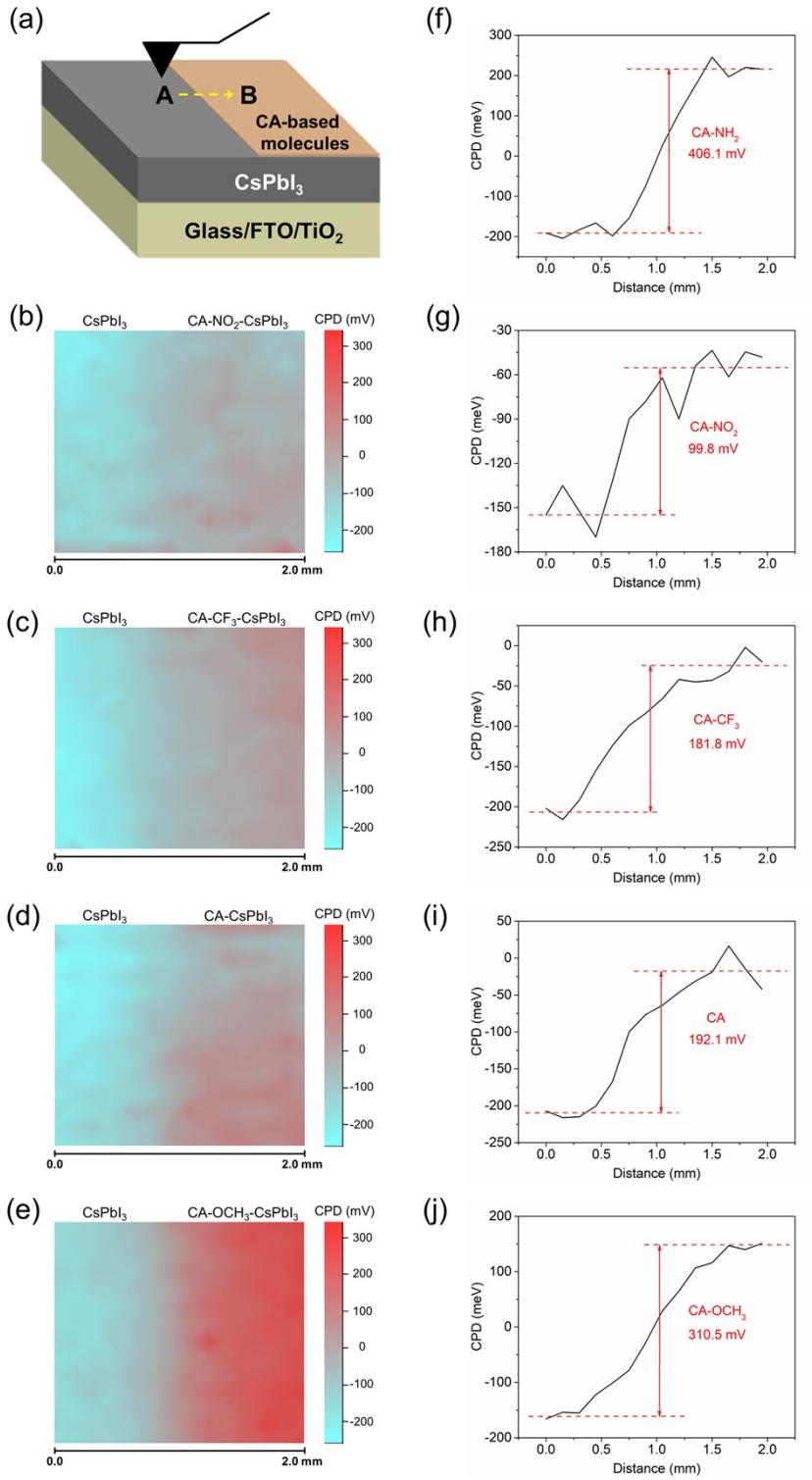

Figure S11. The electric dipole moment of the CA-based molecules interlayer probed by SKPM. a) Schematic diagram of the experimental setup of SKPM. Only the right half part of the perovskite films was treated with CA-based molecules. (b-e) The surface potential spectra of pristine and CA-based perovskite films. (f-j) The cross-sectional profile of the surface potential for pristine and CA-based perovskite films with a direction from A point to B point.

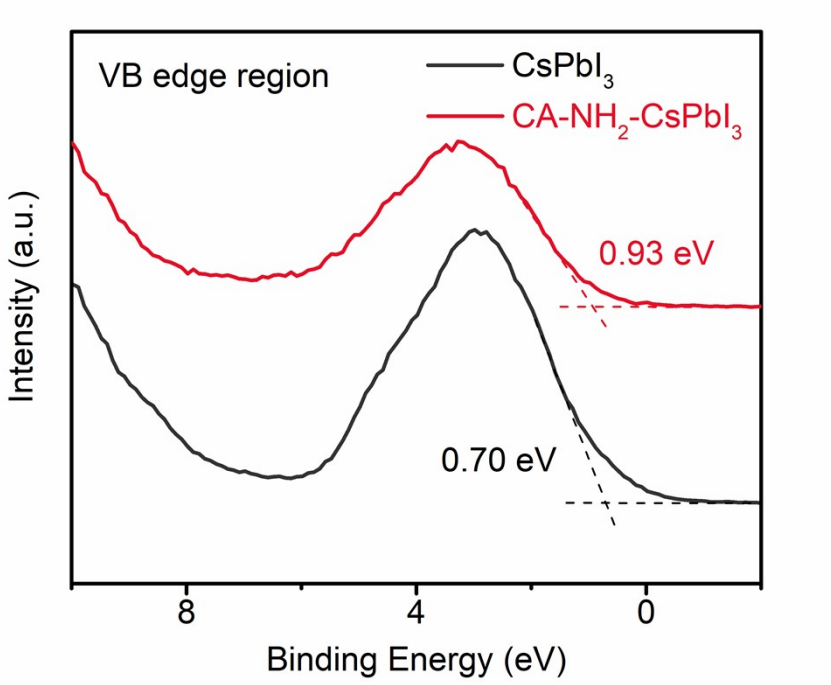

Figure S12. XPS valence band spectra of pristine and CA-NH_2-based perovskite films.

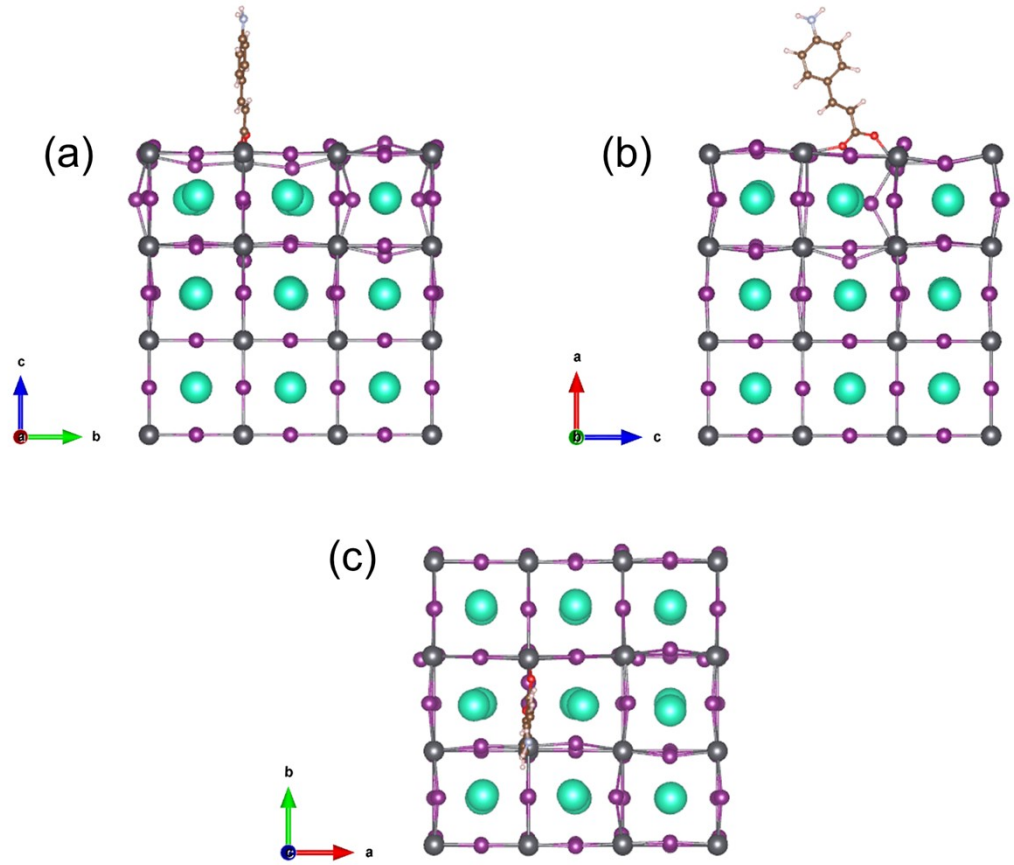

Figure S13. Equilibrated structure of the surface-functionalized perovskite using CA-NH_2 molecules. (a) front view, (b) side view and (c) top view.

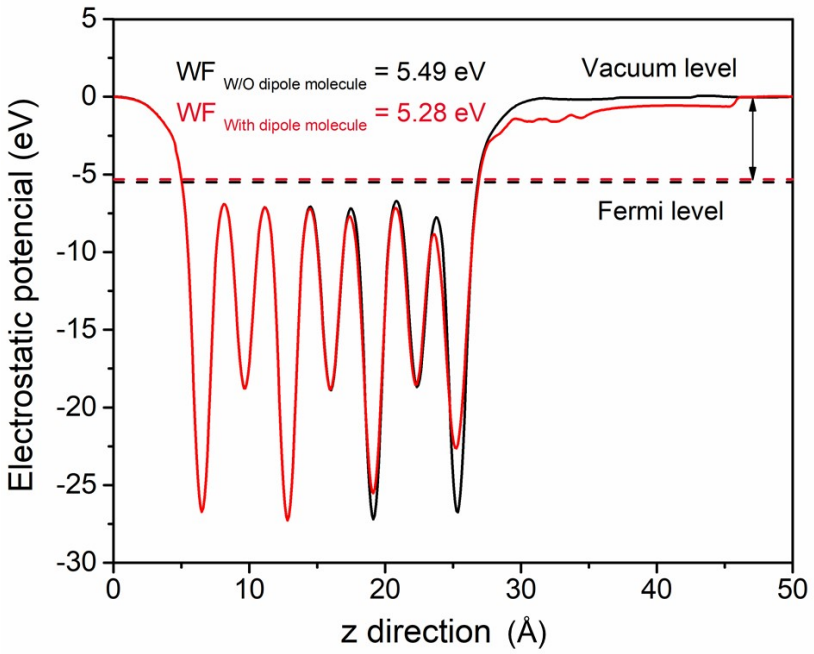

Figure S14. Electrostatic potential of perovskite surface without and with CA-NH_2 molecule.

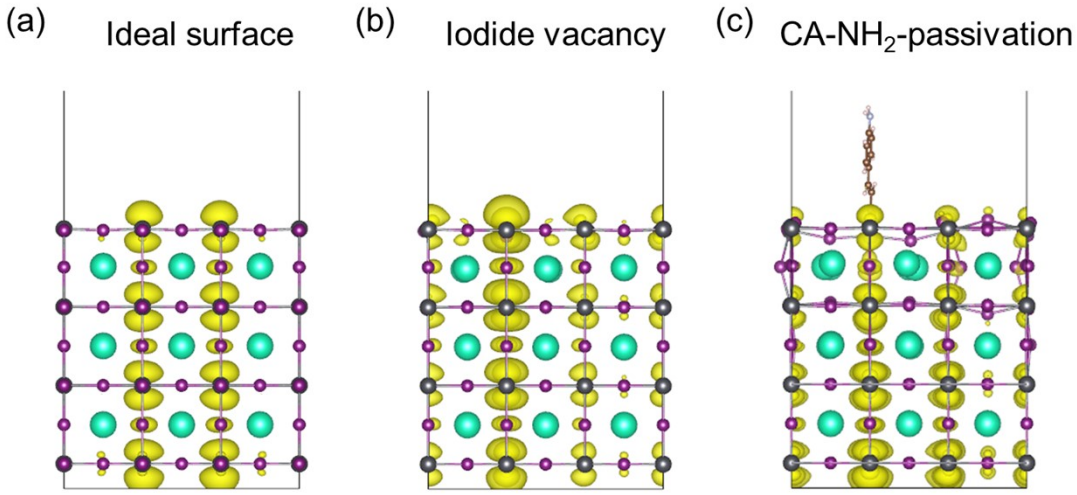

Figure S15. Partial electron density (front view) at the CBM of (a) the ideal perovskite surface, (b) the perovskite surface with V_I and (c) the perovskite surface passivated with the CA-NH_2 molecule with isosurface level equaling to 0.0001 e/Å^3.

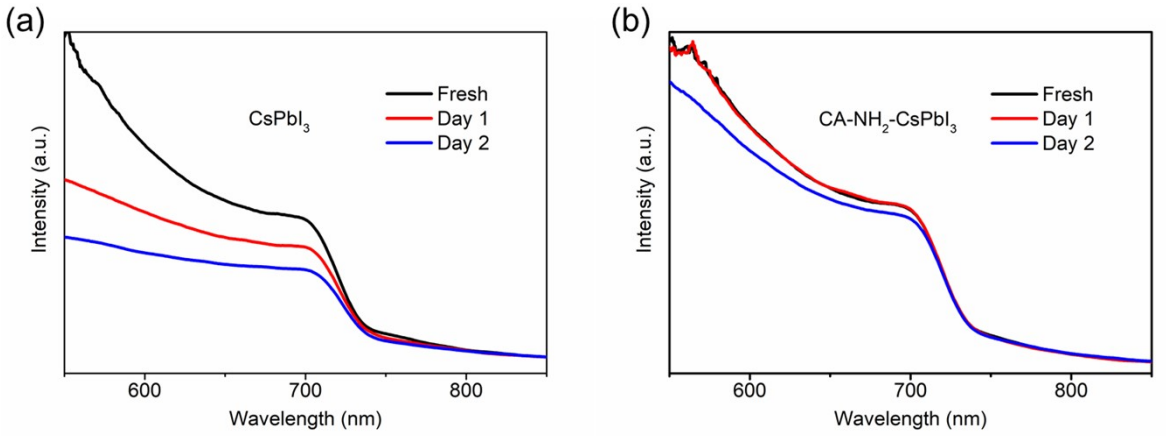

Figure S16. Light absorption spectra of (a) pristine and (b) CA-NH_2-based perovskite films. The perovskite films were stored under ambient conditions at 25 ℃ and RH of 35±5%.

Supporting Tables

Table S1. Photovoltaic performance of CA-NH_2-based $CsPbI_3$ PSCs. The perovskite film was treated with different molecular concentrations.

Sample	V_{oc} (V)	J_{sc} (mA/cm^2)	FF (%)	PCE (%)
Pristine	1.08	19.80	75.5	16.15
2.5 mM	1.12	20.27	80.3	18.24
5 mM	1.16	20.13	81.5	19.03
10 mM	1.10	20.38	78.9	17.69

Table S2. Photovoltaic performance of the PSCs without and with the CA-NH_2 treatment with different voltage scanning directions.

	V_{oc} (V)	J_{sc} (mA/cm^2)	FF (%)	PCE (%)
$CsPbI_3$-Reverse	1.08	19.80	75.5	16.15
$CsPbI_3$-Forward	1.04	19.70	72.1	14.78
CA-NH_2-$CsPbI_3$-Reverse	1.16	20.13	81.5	19.03
CA-NH_2-$CsPbI_3$-Forward	1.11	20.03	80.9	17.98

Table S3. TRPL fitted parameters of pristine and CA-NH_2-based perovskite films.

Sample	A	τ_1 (ns)	B	τ_2 (ns)	$\tau_{(avg)}$ (ns)
Pristine	0.670	10.17	0.322	47.58	36.06
CA-NH_2	0.608	13.32	0.338	130.40	112.22

The PL decay was fitted using a biexponential decay function:[8]

$$I_{PL} = A\exp\left(-\frac{t}{\tau_1}\right) + B\exp\left(-\frac{t}{\tau_2}\right) + C \quad (1)$$

where A, B, and C are constants, t is PL decay time, τ_1 and τ_2 are fitted lifetimes. The average lifetime (τ_{ave}) was calculated using the following equation:

$$\tau_{ave} = \frac{A\tau_1^2 + B\tau_2^2}{A\tau_1 + B\tau_2} \quad (2)$$

Table S4. TPV fitted parameters of pristine and CA-NH_2-based PSCs.

Sample	A	τ_1 (ms)	B	τ_2 (ms)	$\tau_{(avg)}$ (ms)
Pristine	0.557	0.146	0.397	0.468	0.370
CA-NH_2	0.154	0.281	0.773	0.737	0.705

The V_{OC} decay was fitted using a biexponential decay function:[9]

$$V_{OC} = A\exp\left(-\frac{t}{\tau_1}\right) + B\exp\left(-\frac{t}{\tau_2}\right) + C \quad (3)$$

where A, B, and C are constants, t is V_{OC} decay time, τ_1 and τ_2 are fitted lifetimes. The average lifetime (τ_{ave}) was calculated using the following equation:

$$\tau_{ave} = \frac{A\tau_1^2 + B\tau_2^2}{A\tau_1 + B\tau_2} \quad (4)$$

Table S5. EIS parameters of pristine and CA-NH_2-based PSCs.

Sample	R_s (Ω)	R_{res} (Ω)	C_{res}（F）
Pristine	14.79	539	3.22E^{-8}
CA-NH_2	27.26	994	2.59E^{-8}

Supporting Reference

1 G. Kresse and J. Furthmüller, *Comput. Mater. Sci.*, 1996, **6**, 15-50.

2 P. E. Blochl, *Phys. Rev. B-Condens Matter*, 1994, **50**, 17953-17979.

3 S. Grimme, *J. Comput. Chem.*, 2006, **27**, 1787-1799.

4 X. G. Zhao, J. H. Yang, Y. Fu, D. Yang, Q. Xu, L. Yu, S. H. Wei and L. Zhang, *J. Am. Chem. Soc.*, 2017, **139**, 2630-2638.

5 J. Xu, J. B. Liu, B. X. Liu, J. F. Wang and B. Huang, *Adv. Funct. Mater.*, 2019, **29**, 1805870.

6 W.-J. Yin, H. Chen, T. Shi, S.-H. Wei and Y. Yan, *Adv. Electron. Mater.*, 2015, **1**, 1500044.

7 S. Grimme, J. Antony, S. Ehrlich and H. Krieg, *J. Chem. Phys.*, 2010, **132**, 154104.

8 J. H. Liu, Q. S. Zhou, N. K. Thein, L. Tian, D. L. Jia, E. M. J. Johansson and X. L. Zhang, *J. Mater. Chem. A*, 2019, **7**, 13777-13786.

9 X. Zhang, J. Zhang, D. Phuyal, J. Du, L. Tian, V. A. Öberg, M. B. Johansson, U. B. Cappel, O. Karis, J. Liu, H. Rensmo, G. Boschloo and E. M. J. Johansson, *Adv. Energy Mater.*, 2018, **8**, 1702049.